atmosphere

MDPI

Article

Reduced Temperature Sensitivity of Maximum Latewood Density Formation in High-Elevation Corsican Pines under Recent Warming

Philipp Römer [1,*], Claudia Hartl [1], Lea Schneider [2,3], Achim Bräuning [4], Sonja Szymczak [4], Frédéric Huneau [5,6], Sébastien Lebre [7], Frederick Reinig [1], Ulf Büntgen [8,9,10,11] and Jan Esper [1,10]

1 Department of Geography, Johannes Gutenberg-University Mainz, 55099 Mainz, Germany; c.hartl@geo.uni-mainz.de (C.H.); freinig@uni-mainz.de (F.R.); esper@uni-mainz.de (J.E.)
2 Department of Geography, Justus-Liebig-University, 35390 Giessen, Germany; lea.schneider@geogr.uni-giessen.de
3 Center for International Development and Environmental Research, Justus-Liebig-University, 35390 Giessen, Germany
4 Department of Geography and Geosciences, Friedrich-Alexander University Erlangen-Nürnberg, 91058 Erlangen, Germany; achim.braeuning@fau.de (A.B.); sonjaszy@yahoo.de (S.S.)
5 Département d'Hydrogéologie, Université de Corse Pascal Paoli, Campus Grimaldi, BP 52, 20250 Corte, France; huneau@univ-corse.fr
6 Centre National de la Recherche Scientifique, UMR 6134, SPE, 20250 Corte, France
7 Office National des Forêts, 20250 Corte, France; sebastien.lebre@onf.fr
8 Department of Geography, University of Cambridge, Cambridge CB2 3EN, UK; ulf.buentgen@geog.cam.ac.uk
9 Swiss Federal Research Institute, 8903 Birmensdorf, Switzerland
10 Global Change Research Centre, 60300 Brno, Czech Republic
11 Department of Geography, Masaryk University, 61300 Brno, Czech Republic
* Correspondence: phiroeme@uni-mainz.de; Tel.: +49-6131-3929891

Abstract: Maximum latewood density (MXD) measurements from long-lived Black pines (*Pinus nigra* spp. *laricio*) growing at the upper treeline in Corsica are one of the few archives to reconstruct southern European summer temperatures at annual resolution back into medieval times. Here, we present a compilation of five MXD chronologies from Corsican pines that contain high-to-low frequency variability between 1168 and 2016 CE and correlate significantly ($p < 0.01$) with the instrumental April–July and September–October mean temperatures from 1901 to 1980 CE (r = 0.52−0.64). The growth–climate correlations, however, dropped to −0.13 to 0.02 afterward, and scaling the MXD data resulted in a divergence of >1.5 °C between the colder reconstructed and warmer measured temperatures in the early-21st century. Our findings suggest a warming-induced shift from initially temperature-controlled to drought-prone MXD formation, and therefore question the suitability of using Corsican pine MXD data for climate reconstruction.

Keywords: dendroclimatology; tree-ring density; climate signals; *Pinus nigra*; climate change; Mediterranean; France

Citation: Römer, P.; Hartl, C.; Schneider, L.; Bräuning, A.; Szymczak, S.; Huneau, F.; Lebre, S.; Reinig, F.; Büntgen, U.; Esper, J. Reduced Temperature Sensitivity of Maximum Latewood Density Formation in High-Elevation Corsican Pines under Recent Warming. *Atmosphere* **2021**, *12*, 804. https://doi.org/10.3390/atmos12070804

Academic Editors: Jeong-Wook Seo and Masaki Sano

Received: 26 May 2021
Accepted: 15 June 2021
Published: 22 June 2021

1. Introduction

Southern Europe is predicted to experience increasing aridity in the 21st century mainly due to rising temperatures [1–3], and the intensity, frequency, and duration of heatwaves and droughts are expected to increase [4,5]. The precise assessment of climate changes requires proxy-based reconstructions of pre-instrumental conditions to place recent changes into a long-term context. The employment of trees as high-resolution natural climate archives can provide such valuable insights into past climate fluctuations [6]. Although ancient trees growing under extreme conditions and still preserved in their natural state are difficult to find, dendroclimatic studies in Corsica offer the opportunity to reconstruct southern European climate variability over several centuries [7–9].

Located in the central-western Mediterranean region (Figure 1a), Corsica is characterized by strong elevational gradients between the coastal plains and the central mountain massif (Figure 1b). Due to the island's steep relief, altitude-dependent local climate regimes can be observed [10,11]. Coastal regions are characterized by typical Mediterranean climate with hot dry summers (June–August) and temperate rainy winters (October–April). Meteorological observations along the coast record an annual mean temperature of 15.1 °C and precipitation sums of 694 mm from 1961–1990 CE (Figure 1c), with the driest conditions in July (22.7 °C and 12 mm). Over recent decades (1951–2016 CE), a warming trend has been observed which is higher in the June–August summer season (+0.035 °C/year) than in the December–February winter season (+0.014 °C/year) and has been stronger since 1980 CE [12]. With increasing elevation, the temperature generally decreases by 0.31–0.49 °C/100 m and precipitation increases by approx. 160 mm/100 m [11]. However, spatial precipitation patterns are strongly influenced by topographical features and are, thus, geographically much more diverse than temperature. Although precipitation generally increases with altitude, high elevation areas can be subject to severe droughts during summer, especially between July–August. Consequently, the Corsican mountains can be characterized as xeric in summer and alpine in winter [13].

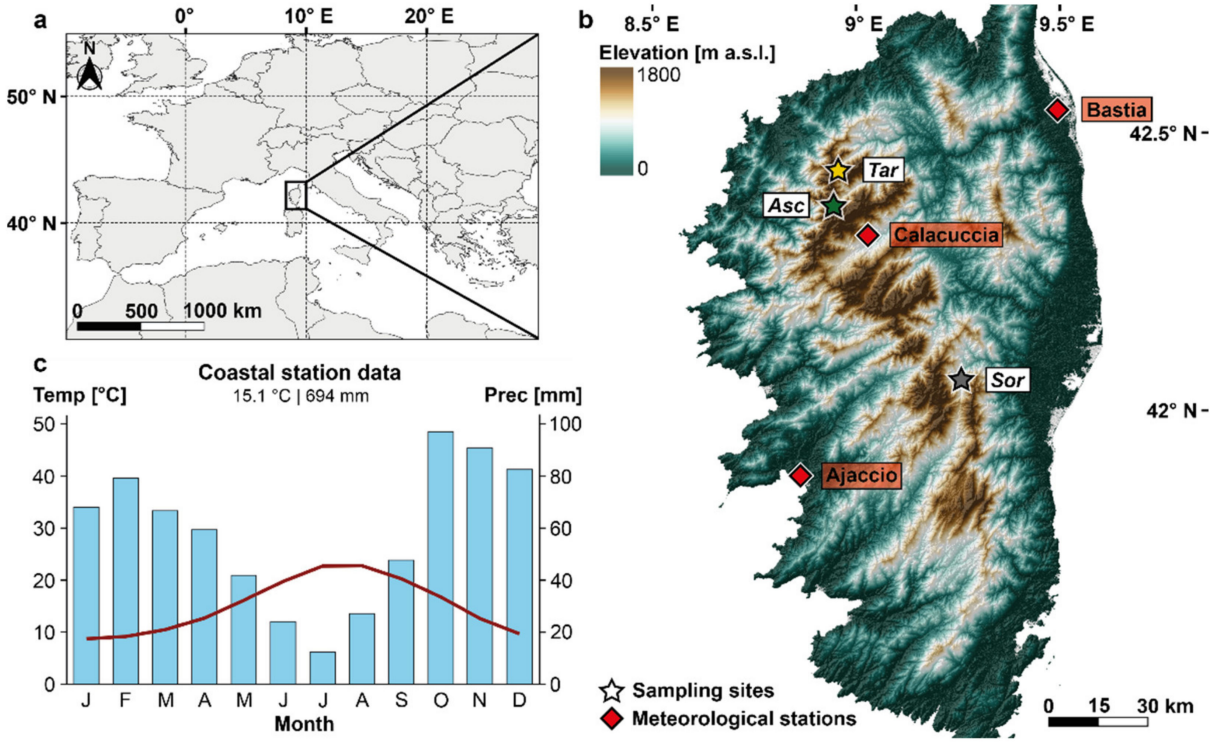

Figure 1. Study site and climate. (**a**) Geographical location of Corsica in the Mediterranean. (**b**) Topographic map of Corsica indicating the sampling sites and meteorological stations. (**c**) Climate diagram showing monthly temperatures (red curve) and precipitation (blue bars) of the combined station data from Ajaccio and Bastia (1961–1990 CE).

Due to the great variety of microclimates, the Corsican mountains feature a high ecological biodiversity [14] including two native pine species: Maritime pine (*Pinus pinaster* AITON) and Corsican Black pine (*Pinus nigra* ssp. *laricio* MAIRE). The former mainly covers lower elevations <1300 m a.s.l. that are strongly influenced by anthropogenic activities. In contrast, Black pine forests are in the high elevation belt between 1400–1800 m with remnants of natural stands near the upper treeline (Figure 2a).

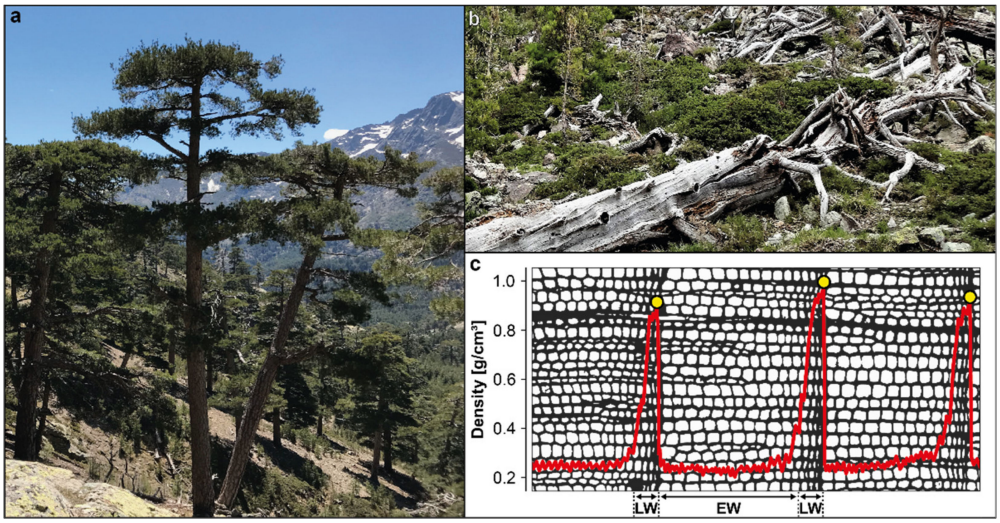

Figure 2. Corsican pines and wood density. (**a**) Living trees and (**b**) relict trunks of *Pinus nigra* at the upper treeline in the Asco valley. (**c**) Thin section of three tree rings and the density profile (red curve) across the earlywood (EW) and latewood (LW). Yellow dots indicate the maximum latewood density (MXD).

The drought- and frost-tolerant *P. nigra* [15,16] may reach ages up to 850 years [7], ranking these trees among the oldest in the Mediterranean Basin [17]. Particularly resistant to parasites and decomposition due to their high resin content [18], relict pine stems can remain for centuries on the rocky slopes (Figure 2b). The presence of these well-preserved trunks in the vicinity of old living stands offers the opportunity to develop multi-centennial tree-ring chronologies.

In drought-dominated regions, tree-growth is typically determined by the availability of water resulting from the mutual interaction of temperature, precipitation, and evapotranspiration [19,20]. Due to low water supply in summer, Mediterranean forest productivity is dependent on the frequency and amount of rainfall events before and during the growing season. Consequently, tree-ringwidth (TRW) chronologies have been used as proxies to reconstruct precipitation [21–24] and hydroclimatic variability across southern Europe [25–29]. High-resolution summer temperature reconstructions are restricted to other tree-ring parameters, such as the maximum latewood density (MXD), as the TRW is less temperature sensitive in Mediterranean environments [30].

MXD chronologies are generally less influenced by biological memory effects and correlate more closely with instrumental temperature data [31]. However, compared to the extensive networks in Fennoscandia [32,33] and the Alps [34], the availability of temperature-sensitive density records spanning 500+ years in the Mediterranean is restricted to the Spanish Central Pyrenees [35,36], the Cazorla Natural Park in southern Spain [37], and the Pindos National Park in north-western Greece [38,39]. With respect to the central Mediterranean region, comparably long-term MXD chronologies are still missing.

Nonetheless, two annually resolved temperature reconstructions provide initial insight into the region's past climate variability: Leonelli et al. [40] developed a 300-year temperature reconstruction based on a multi-site MXD network in Italy, while the only temperature reconstruction for Corsica was derived from stable carbon isotopes ($\delta^{13}C$) extending 560 years into the past [8]. Hence, a long-term MXD-based temperature reconstruction from Corsica is still lacking and remains key to unfold the region's climate history into the early second millennium.

Here, we present the longest MXD record for the Central-Western Mediterranean based on 35 *P. nigra* trees growing at three high-elevation sites on the island of Corsica (France). Covering the period 1168–2016 CE, the dataset extends existing MXD measurements (1518–1980 CE) [41] back to medieval times as well as into the 21st century. To

evaluate the application of Regional Curve Standardization (RCS), age-band chronologies were produced and different chronology variants were correlated against regional climate data. In this study, we (1) assess climate signals in five chronology variants of the new Corsican MXD compilation, (2) compare new density data with existing records and summer temperature reconstructions across the southern European region, and (3) evaluate the potential of the Corsican MXD network for climate reconstruction.

2. Materials and Methods

2.1. Wood Density Data and Chronology Development

In 2017, 39 increment cores from 20 living and relict Black pines (*Pinus nigra* ssp. *laricio*) were sampled at two high-elevation sites in the adjacent Asco (*Asc*, 1600 m a.s.l.) and Tartagine valleys (*Tar*, 1450 m a.s.l.), located near the upper treeline in the north-western mountains of Corsica (Figure 1b). Long-lived trees from these valleys were previously used to develop multi-centennial tree-ring records [7–9]; however, no wood density measurements have been performed. To obtain the longest possible time series, mainly old and dominant trees as well as cross-dated relict stems were selected for this study.

Following standard radio-densitometric techniques [42–44], all cores were heated in 96% ethanol in a Soxhlet extraction system to remove the hydrophobic components. The purified samples were split into 3-cm segments to saw out 1.2-mm thick laths orthogonally to the longitudinal stem axis. The laths were acclimatized at 20 °C and 50% relative humidity for 4 h to ensure a homogeneous cell wall moisture content of ~10%. Subsequently, the samples were radiographed for 14 min at 10 kV and 20 mA and the wood densities determined at 0.01 g/cm^3 resolution using a Walesch high-precision DENDRO2003 X-ray densitometer. The density peaks in each tree ring were used to produce inter-annual MXD data (Figure 2c).

After aligning the MXD data by cambial age, a Hugershoff-shaped age trend was observed, including an average increase of 0.1 g/cm^3 over the first 70 years of growth and a gradual decrease of 0.13 g/cm^3 over the subsequent 330 years (71–400 years). To remove this characteristic biological trend from the raw MXD data [32,33], a Hugershoff Standardization (HGS) and a Regional Curve Standardization (RCS) were applied in the detrending program ARSTAN [45], resulting in two chronology variants: COR_{HGS} and COR_{RCS}.

After applying a data adaptive power-transformation to minimize heteroscedasticity within the individual series [46], all data were detrended by calculating residuals from the smoothed HGS-/RCS-mean curves and variance-stabilized using a 300-year spline with a fixed 50% cutoff to avoid deviations caused by changing sample replications and inter-series correlations [47]. Robust bi-weight mean chronologies were computed [48] and the covariance of each chronology was assessed by calculating the inter-series correlation (Rbar) and the Expressed Population Signal (EPS) over semi-overlapping 30-year periods [49].

The new density data produced in our laboratory in Mainz (Germany) were compared with older measurements (n = 30 series), produced in the early 1980s in Birmensdorf (Switzerland) covering the period 1518–1980 CE [41] (data available from the International Tree-Ring Data Bank, www.ncdc.noaa.gov/data-access/paleoclimatology-data, accessed on 5 October 2020). The latter were derived from Black pines growing at the mountain pass Col de Sorba on Monte Renoso (*Sor*, 1400 m a.s.l.), which is located ~45 km southeast of the new sites (Figure 1b). Given the significant correlation (r_{avg} = 0.46) among the three site chronologies *Asc*, *Tar,* and *Sor* from 1636 to 1980 CE (Figure 3, see Supplementary Table S1 for detailed site chronology characteristics), we produced a merged dataset integrating all Corsican MXD data (*COR*).

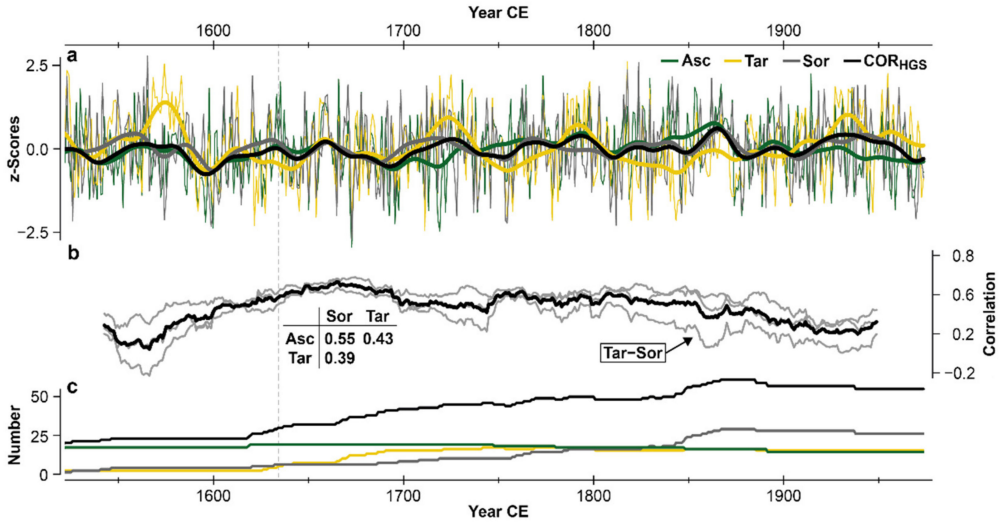

Figure 3. (**a**) Hugershoff-detrended MXD composite (COR_{HGS}) and site chronologies (*Asc*, *Tar*, and *Sor*) (thin curves) and their 31-year smoothing splines (bold curves). (**b**) The 51-year running correlations between the site chronologies (grey) shown together with their mean (black). The inserted table indicates inter-site correlations calculated over the sufficiently replicated ($n \geq 5$ series) common period 1636–1980 CE (1636 CE is marked by a vertical dashed line). (**c**) Sample replication of each chronology.

The composite dataset contained 69 MXD series and exceeded a robust EPS of ≥0.85 back to 1425 CE (Figure S1). When merging the data, the absolute MXD values were adjusted among the sites to mitigate significant ($p < 0.001$) elevational MXD effects between *Tar* and *Sor* (0.96 g/cm^3) and *Asc* (0.89 g/cm^3) calculated for the first 200 years of growth (Figure S2).

Both detrending techniques applied in this study—HGS and RCS—are able to preserve multi-centennial variability in dimensionless index chronologies [50,51], although HGS is an individual detrending method and is restricted by the "segment length curse" [52]. Accurate RCS detrending, however, requires the mean cambial age of the series combined in a chronology to be constant over time [53,54]. To avoid the typical increase in mean tree age toward the present, age-band chronologies (*ABC*) [55] were produced by removing tree rings younger than 30 years and older than 200 years (*ABC200*), 300 years (*ABC300*), and 400 years (*ABC400*) of cambial age (see Supplementary Table S2 for chronology characteristics). Accordingly, five methodologically different chronologies were developed considering HGS and RCS with all data, as well as RCS with three age bands: COR_{HGS}, COR_{RCS}, *ABC200*, *ABC300*, and *ABC400*.

2.2. Climate Data and Signal Estimation

To assess the climate sensitivity of Corsican Black pine MXD and evaluate its suitability for reconstruction purposes, climate data from the meteorological stations in Ajaccio (41.92° N, 8.80° E, 9 m a.s.l.) and Bastia (42.54° N, 9.49° E, 10 m a.s.l.), CRU TS4.04 temperature data [56], and GPCC v2020 precipitation data [57] were compiled using the KNMI Climate Explorer [58]. The selected CRU and GPCC grids extended across 42–42.5° N and 8.5–9.5° E, covering the entire study area.

The GPCC data were chosen for the analysis of precipitation signals due to the high station density in Europe and long temporal coverage back to 1891 CE [57]. The temperature means and precipitation totals were converted into monthly and seasonal anomalies with respect to 1961–1990 CE. The observations from Ajaccio and Bastia were merged by calculating the arithmetic means from 1951 to 2016 CE. Comparison of the coastal station means with recordings from a local higher station in Calacuccia (875 m a.s.l.,

42.34° N and 9.01° E) back to 1975 CE [59] revealed 3.76 °C warmer conditions from April to October in Ajaccio and Bastia.

The local temperatures are, however, closely correlated with the coastal records (r = 0.86) and CRU temperatures (r = 0.84). In contrast, the annual precipitation totals from Calacuccia were less correlated with the coastal records (r = 0.53) and GPCC data (r = 0.67). We, therefore, used the coastal means and CRU temperatures as well as the GPCC precipitation data to assess the climate sensitivity of high-elevation MXD records.

All MXD chronologies were correlated (Pearson's r) with monthly and seasonal climate data over the 1951–1980 CE period to compare the climate signals contained in the old and new density measurements, as well as over the 1951–2016 CE period to account for recent climate variability. To evaluate the temporal robustness of the climate signals, 31-year running correlations were calculated between the density indices and different seasonal averages of meteorological data (April–July and September–October temperatures as well as June–July and August–September precipitation). Further, all MXD chronologies were correlated with 0.5° gridded monthly and seasonal CRU TS4.04 data using the KNMI Climate Explorer to assess spatial correlation patterns over the Mediterranean Basin from 37–47° N and −3–21° E.

3. Results

3.1. MXD Chronology Characteristics

The *COR* MXD compilation consists of 69 radii from 35 pine trees and spans the period 1168–2016 CE, including an increasing number of measurements toward the present (Figure 4). Replication falls below five series at 1359 CE, while the maximum of 61 series is reached from 1872 to 1890 CE. *COR* replication decreases again in the late 20th century from 55 series in 1980 CE to 29 series in 1981 CE, when the *Sor* data terminate. Over the first 400 years of cambial age, average MXD (AMXD) is 0.91 g/cm^3 (±0.05 g/cm^3) with a minimum of 0.78 g/cm^3 in the fifth year of growth and a maximum of 1.00 g/cm^3 in the 107th year of growth. This juvenile AMXD increase is followed by a small but persistent decrease (Figure S3).

The lengths of the individual series ranged from 67 to 849 years with a mean segment length (MSL) of 325 years, whereas the age classes are unevenly distributed across the sites. Trees sampled at the *Asc* site were significantly ($p < 0.01$) older (MSL_{Asc} = 543 years) than those at the two lower sites (MSL_{Tar} = 290 and MSL_{Sor} = 211 years). Consequently, *COR* was characterized by a heterogenous age structure and site composition over time. All five *COR* chronologies shared annual to multi-decadal scale variability. Further, COR_{HGS} showed a significant ($p < 0.001$) agreement in correlation with the site chronologies (r = 0.67–0.82) over the sufficiently replicated ($n \geq 5$ series) 1636–1980 CE common period.

Compared to *COR*, the age-band chronologies—*ABC200*, *ABC300*, and *ABC400*—were characterized by flatter mean age and replication curves (Figure 4b–f). Due to the removal of tree rings older than 200, 300, and 400 years (and younger than 30 years) the age-band chronologies cover different periods. Whereas all chronologies extend back to 1365 CE with $n \geq 5$ series, *ABC200* already ends in 1980 CE, *ABC300* in 1988 CE, and only *ABC400* reaches into the 21st century until 2016 CE. Inter-chronology differences in replication and site contributions, thus, increase toward the present.

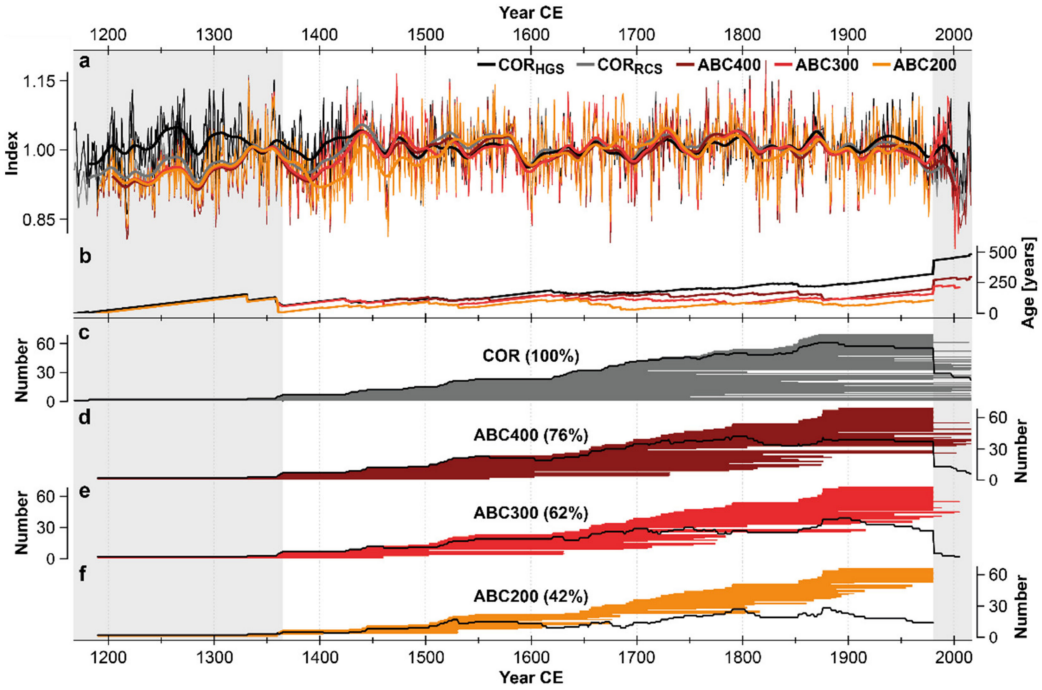

Figure 4. Effects of age-band decomposition. (**a**) Detrended composite chronologies (thin curves) and their 31-year smoothing splines (bold curves) considering all MXD data (*COR*), data from 30–400 years (*ABC400*), 30–300 years (*ABC300*), and 30–200 years (*ABC200*). COR was detrended using HGS (COR_{HGS}) and RCS (COR_{RCS}), while all age-band chronologies were detrended using RCS. (**b**) The mean tree age of the chronologies. (**c**–**f**) Samples (bar plots) and replication (black lines) of the chronologies. Each horizontal bar depicts one individual series. The percentages in brackets indicate the remaining data compared to *COR* (=100%). Grey-shaded areas mark the periods when replication in at least one record is $n < 5$ series.

The age-band chronologies showed substantial agreement in high-to-low frequency covariance ($r_{avg} = 0.91$) and correlated significantly at $r_{avg} = 0.92$ with the untruncated chronology COR_{RCS} over the well-replicated ($n \geq 5$ series) 1365–1980 CE common period. On multi-decadal scales, MXD indices of all chronologies increased from around 1400 to 1440, 1600 to 1660, 1700 to 1730 and 1760 to 1790 CE, and decreased from 1360 to 1390, 1440 to 1460, 1580 to 1600, 1730 to 1760, 1790 to 1820, 1860 to 1910 and 1950 to 1980 CE.

In the 20th century, however, the smoothed chronologies diverged considerably: COR_{RCS} and *ABC400* both showed a minor increase from 1975–1990 CE and a sharp decline thereafter; the smoothed *ABC300* ends in 1990 CE and showed a striking post-1975 CE increase due to low sample replication; while *ABC200* only extends until 1980 CE and showed no remarkably deviations from the other chronologies in the 20th century, but did in periods of $n < 10$ series, such as the late 17th century and before ~1510 CE. Furthermore, large differences were observed between the HGS- and RCS-indices prior to ~1425 CE, as evidenced by a downward shift in the RCS-values in the earliest density measurements. These differences were slightly higher between the COR_{HGS} and the age-bands than between the COR_{HGS} and COR_{RCS}.

The comparison of COR_{HGS} with other long-term density records from southern Europe revealed a generally decreasing correlation with increasing geographic distance (Table 1, Figure 5a). COR_{HGS} correlated significantly ($p < 0.001$) with the pine MXD records from the Spanish Central Pyrenees (*GER*, r = 0.53) [35] and southern Italy (*CRI*, r = 0.42) [60] from 1360–2004 CE, while weaker associations were found with more distant (>1000 km) records from southern Spain (*CAZ*, r = 0.33) [37] and north-eastern Greece (*SMO*, r = 0.28) [38]. Correlations with western Mediterranean sites were slightly higher than with equidistant sites in the eastern Mediterranean.

Table 1. Characteristics of the Mediterranean MXD records.

Code	Site	Species	Radii	Period	Season	Correlation	Distance
CAZ	Cazorla	PINI	88	1288–2014	FMAM and SO	0.53 | 0.45	1150 km
COR	Corsica	PINI	69	1360–2016	AMJJ and SO	0.56 | 0.16	0 km
CRI	Serra di Crispo	PIHE	21	1604–1980	JAS	0.60 | 0.60	650 km
GER	Gerber	PIUN	414	1095–2014	MJ and AS	0.59 | 0.38	650 km
LOE	Loetschental	LADE	180	748–2004	JJAS	0.77 | 0.78	450 km
SMO	Mt. Smolikas	PIHE	192	672–2017	AS	0.52 | 0.56	1050 km

Species: LADE: *Larix decidua*, PIHE: *Pinus heldreichii*, PINI: *Pinus nigra*, and PIUN: *Pinus uncinata*. Period: Start and end dates were set considering a sample replication of ≥5 radii. Correlation: Pearson correlations of HGS-detrended MXD chronologies calibrated against nearby seasonal CRU TS4.04 temperatures over the 1901–1980 CE common period (left value) and from 1901 to the actual end date of each chronology (right value). Distance: Linear distance from Corsica.

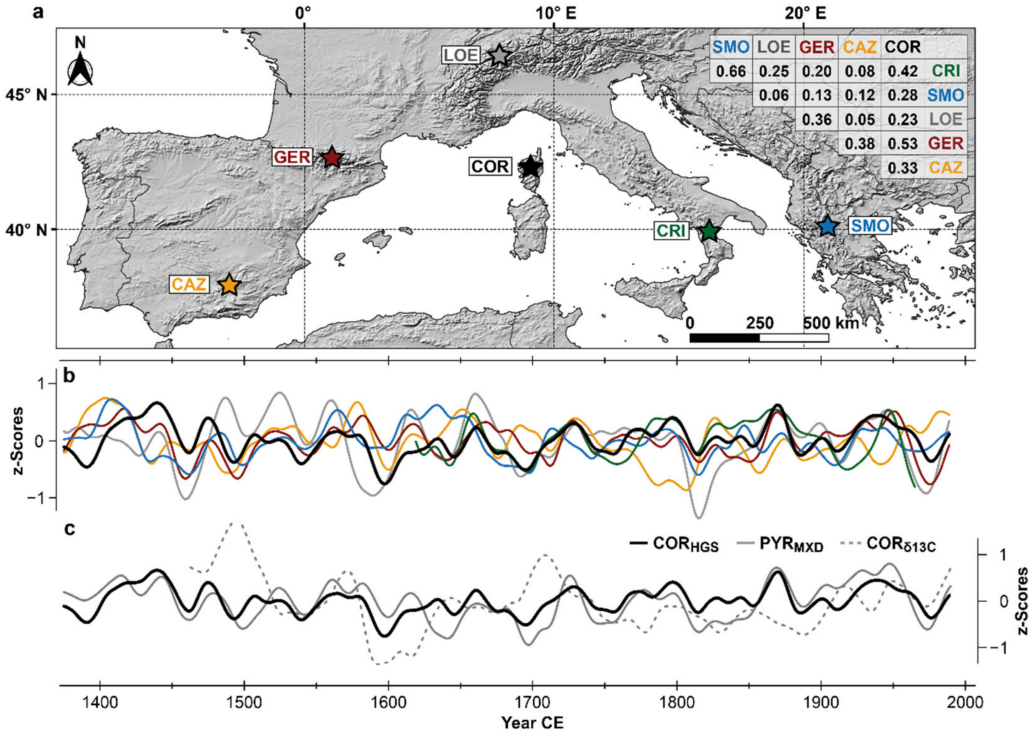

Figure 5. Comparison of the long MXD chronologies from southern Europe. (**a**) Location of the MXD sites: Cazorla (*CAZ*), Gerber (*GER*), Corsica (*COR*), Serra di Crispo (*CRI*), and Mt. Smolikas (*SMO*). The matrix shows correlations between the HGS-detrended chronologies over their 1360–2004 CE common period—except for *CRI*, which covers a shorter period from 1604–1980 CE. (**b**) The 31-year smoothing splines of the normalized HGS-detrended MXD chronologies from 1375–1989 CE ($n \geq 5$ series). (**c**) COR_{HGS} shown together with the August–September temperature reconstruction from Corsican pine stable carbon isotopes ($COR_{\delta 13C}$) [8] and a May–September temperature reconstruction from the Pyrenees based on MXD (PYR_{MXD}) [36]. All records were normalized (COR_{HGS} and PYR_{MXD} from 1360–2005 and $COR_{\delta 13C}$ from 1448–2005 CE) and smoothed using a 31-year spline.

However, the weakest association was observed with the nearest record from the Swiss Alps (*LOE*, r = 0.23) [34], located only ~450 km north of COR_{HGS}, which is the only chronology based on *Larix decidua* instead of pine species. The smoothed density records from the Mediterranean outline both periods of high and low inter-regional correlations (Figure 5b). High covariance was primarily found in periods of pronounced variability, such as 1440–1500, 1580–1610, 1650–1670, 1810–1830, and 1850–1890 CE, whereby the z-score levels differed among the sites. Moreover, some chronologies indicated substantially deviating behavior, e.g., *CAZ* from 1760–1810 CE.

Further comparison with tree-ring based temperature reconstructions (Figure 5c) from Corsica ($COR_{\delta 13C}$) [8] and the Spanish Pyrenees (PYR_{MXD}) [36] demonstrated that the inter-annual MXD variability of *P. nigra* was more strongly associated with reconstructed May–September temperatures from the Iberian Peninsula ($r_{1582–2005}$ = 0.55) than with reconstructed August–September temperatures from Corsica ($r_{1582–2005}$ = 0.16), although the latter were derived from stable carbon isotopes of six Black pines sampled close to the *COR* sites [8]. In contrast, the reconstruction from the Pyrenees was based on a multiple-site *Pinus uncinata* MXD network [36].

3.2. Climate Sensitivity of Corsican MXD

MXD in Mediterranean conifers was primarily influenced by the warm-season temperatures (Table 1). In Corsica, correlations between the site chronologies and regional observations revealed local differences in temperature sensitivity as well as temporal changes in signal strength (Figure 6). The site chronologies showed weak to moderate associations to the regional April–July and September–October mean temperatures (AMJJ and SO) over the 1951–1980 CE period, ranging from r = 0.17 at *Tar* to r = 0.47 at *Sor*. Although correlations with regional July temperatures were low overall (r = 0.03–0.15), analysis with the CRU temperatures indicated a significant ($p < 0.01$) association of r = 0.42 at *Sor* (Figure S4).

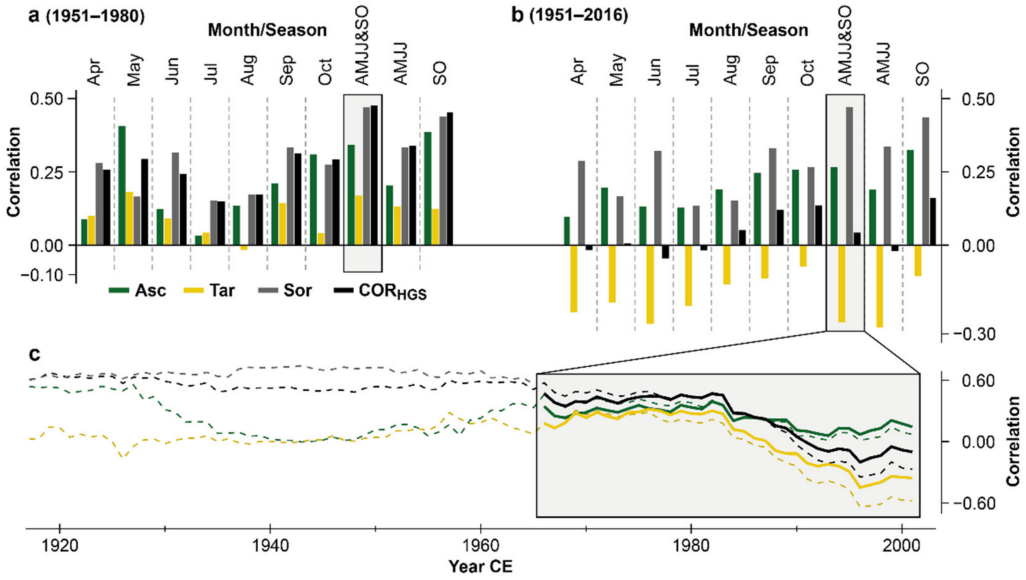

Figure 6. Site-specific temperature signals. Correlations between the Hugershoff-detrended chronologies and monthly and seasonal temperatures of the combined station records from (**a**) 1951–1980 and (**b**) 1951–2016 CE. Note that *Sor* only extends to 1980 CE and indicates same correlations in (**a**) and (**b**). (**c**) The 31-year running correlations between the chronologies and seasonal AMJJ and SO temperatures of the station records (thick solid curves) and CRU data (thin dashed curves). See Supplementary Figure S4 for more detailed correlations with monthly and seasonal CRU temperatures.

The COR_{HGS} composite record showed a similar temperature sensitivity to *Sor*, with the highest correlation found for the AMJJ and SO season (r = 0.47, $p < 0.01$) from 1951 to 1980 CE. Extending the calibration period into the 21st century resulted in a systematic decrease in the temperature sensitivities (Figure 6b). While the *Asc* correlation with AMJJ and SO temperatures marginally weakened from $r_{1951–1980}$ = 0.34 to $r_{1951–2016}$ = 0.27, the originally positive correlation of *Tar* turned negative when extended into the 21st century, from $r_{1951–1980}$ = 0.17 to $r_{1951–2016}$ = –0.26. In line with these *Asc* and *Tar* responses (*Sor* terminates in 1980 CE), a decline toward insignificant temperature correlations was also seen in COR_{HGS} when including the post-1980 CE data ($r_{1951–2016}$ = 0.04).

Thirty-one-year running correlations between the chronologies and seasonal AMJJ and SO temperatures confirmed these findings (Figure 6c): COR_{HGS} indicated a temporally stable temperature signal until 1983 CE against station ($r_{1966–1983}$ = 0.34–0.47) and CRU data ($r_{1916–1983}$ = 0.42–0.67). These results were higher than the observations for *Asc* and *Tar* but slightly lower than *Sor*. However, the running correlations of all chronologies decreased sharply after 1983 CE, and this decline was stronger in *Tar* and weaker in *Asc*, whereas COR_{HGS} remained in-between.

The five MXD composite chronologies all showed similar temperature sensitivities from 1901–1980 CE (Figure 7). Correlations with the April–July CRU temperatures (r = 0.43–0.53) were slightly higher than with the September–October means (r = 0.33–0.44), but the AMJJ and SO season fit best (r = 0.52–0.64). The strongest association with temperature was observed for the most truncated age-band chronology *ABC200* (r = 0.64, $p < 0.01$). Spatial analyses using gridded CRU temperatures revealed strong correlations with the April–October means across the western and central Mediterranean regions (Figure 7a). The highest correlations ($r \geq 0.40$) were found with the June–July temperatures over Corsica, Iberia, and Maghreb.

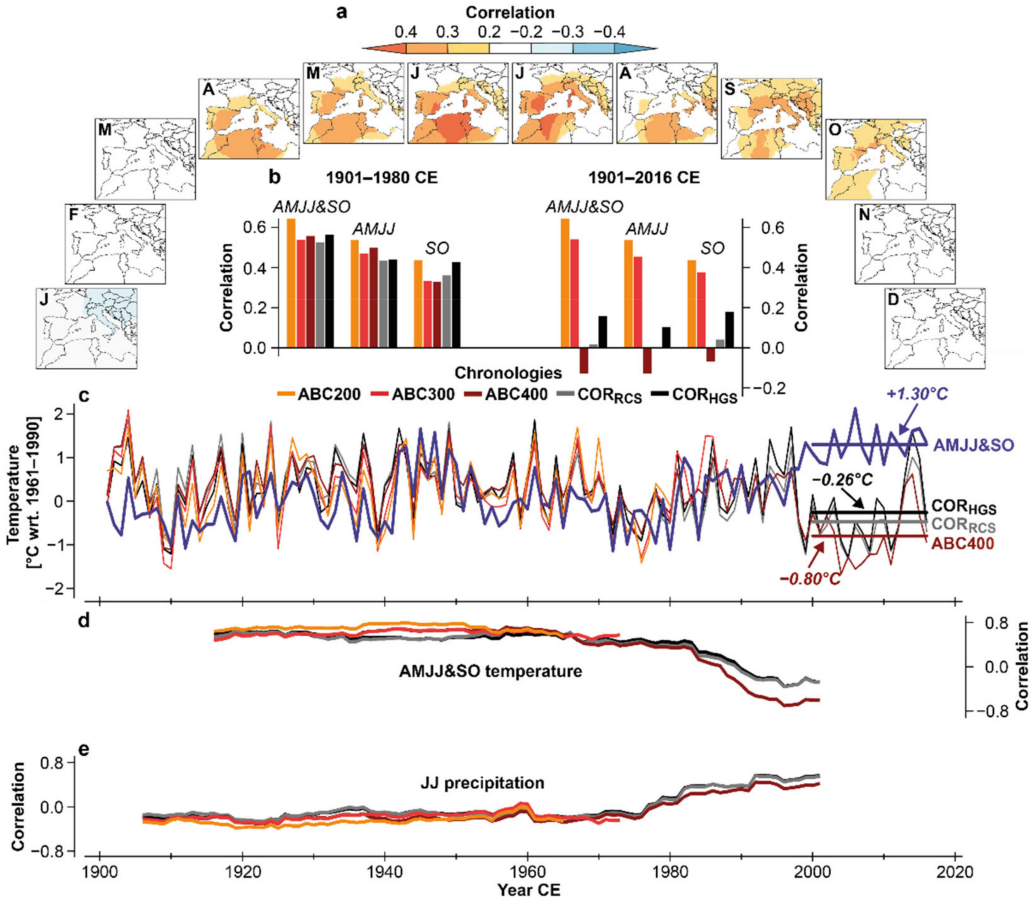

Figure 7. Climate signals of the Corsican composite chronologies. (**a**) Spatial correlations between *ABC200* and 0.5° gridded monthly temperatures (CRU) over the Mediterranean Basin (1901–1980 CE). Significant correlations at $p < 0.1$ are colored. (**b**) Correlations between the composite chronologies and seasonal temperatures from 1901–1980 (left) and 1901–2016 CE (right). Note that *ABC200* and *ABC300* only extend until 1980 and 1988 CE, respectively. (**c**) MXD chronologies scaled from 1901–2016 CE against AMJJ and SO temperature anomalies (CRU). The horizontal lines display the mean temperatures from 2000 to 2016 CE. The 31-year running correlations between the MXD chronologies, (**d**) CRU AMJJ and SO temperatures, and (**e**) GPCC JJ precipitation. See Supplementary Figure S5 for details on the GPCC correlations.

In August, however, correlations over the study area declined (r = 0.21). As for the site chronologies, a systematic decrease in signal strength was observed in the composite records when the calibration period was extended into the 21st century (Figure 7b). All MXD chronologies reaching 2016 CE with $n \geq 5$ series (COR_{HGS}, COR_{RCS}, *ABC400*) showed non-significant low correlations with the AMJJ and SO temperatures over the full 1901–2016 CE period. A simple scaling of COR_{HGS} against post-1900 CE temperatures highlights a substantial divergence of 1.56 °C between the colder reconstructed (t = −0.26 ± 0.78 °C) and warmer measured temperatures (t = +1.30 ± 0.38 °C) from 2000 to 2016 CE, although the MXD and temperature records display similar interannual to decadal scale variability over most of the 20th century (Figure 7c).

The observed 21st century divergence is caused by opposing low-frequency trends starting in the late 1990s and is even greater when considering COR_{RCS} and *ABC400*, respectively. The 31-year running correlations support these findings (Figure 7d), as all composite chronologies showed temporally stable temperature correlations ≥0.45 before 1967 CE, followed by r = 0.30–0.45 from 1968 to 1983 CE and a sharp decrease thereafter. Simultaneously, running correlations with June–July precipitation increased since the 1980s (Figure 7e).

Analyses using the GPCC precipitation data showed that the Corsican composite records were only weakly associated with precipitation (Figure S5). Between 1891 and 1980 CE, all chronologies correlated significantly ($p < 0.05$) negatively with the June–September precipitation (r = −0.28 to –0.36). Correlations were lower and insignificant over the full 1981–2016 CE calibration period for COR_{HGS}, COR_{RCS}, and *ABC400;* however, the running correlations with the June–July precipitation showed a sharp post-1980 CE increase, while the correlations with the August–September precipitation remained stable.

4. Discussion

4.1. Chronology Variants and Characteristics

The combination of MXD data from three different valleys enabled the development of a regional record (*COR*) characterized by a high sample replication ($n = 69$) and a robust common signal (EPS ≥ 0.85) back to 1425 CE. The five methodologically different composite chronologies share high fractions of high-to-low frequency variance from 1500 to 1980 CE. Noticeable trend differences were recorded before ~1500 CE and in the late 20th and early 21st centuries (Figure 4). The age-band datasets more closely meet the requirements for RCS detrending [50,61], as these chronologies are characterized by more balanced replication and age curves.

Thus, our findings imply that age-band decomposition—as introduced by Briffa et al. [55] for a large network of Northern Hemisphere MXD data to improve the preservation of long-timescale variability and successfully applied in recent studies by Esper et al. [33,37]—produces a sample structure that is likely more applicable for RCS detrending. However, the differences between *ABC200*, *ABC300,* and *ABC400* remained small and restricted to periods of weaker sample replications ($n < 10$ series). This is particularly the case in *ABC200*, as this chronology was most affected by the systematic removal of old tree rings.

The substantial data reduction together with the marked discrepancies with all other chronologies during low-replication periods raises questions regarding the overall reliability of *ABC200*. *ABC300* and *ABC400*, on the other hand, are characterized by less variable replication curves. Even after the removal of tree rings older than 400 years, *ABC400* extends until 2016 CE with sufficient data replication. Yet removing data from the comparably small Corsica MXD dataset remains challenging.

Large differences between the HGS and RCS indices before ~1425 CE and smaller deviations after 1900 CE raises doubts regarding the suitability of RCS for our dataset. While HGS, as a tree-by-tree standardization technique, is barely able to preserve multi-centennial variability and produces a quasi-stationary chronology fluctuating around a mean index of one, the composite RCS technique retains more low frequency variance and produces constantly lower values at each chronology end (Figure 4).

Whether these low frequency trends are valid is difficult to estimate; however, we hypothesize that the regional curves established in the RCS runs [50] do not adequately represent the earliest and latest density measurements, particularly during the low-replication period prior to ~1425 CE. This bias might originate from the selective sampling approach that focuses on old living trees and leads to younger trees being underrepresented in all chronologies [62]. However, to clarify these methodological limitations, a larger MXD dataset including different age classes is required.

4.2. Bimodal Temperature Signal

Various studies have reported warm-season temperatures to be the main climatic driver of MXD formation in high-elevation Mediterranean conifers [30,35–40]. Regarding the calibration with pre-1980 CE instrumental data, our results are consistent with these findings revealing significant temperature correlations throughout the growing season from April to October including a lack of forcing in August. In contrast, the influence of precipitation on MXD appears to be minor. The resulting bimodal seasonality of temperature signals is comparable to the findings reported by Büntgen et al. [35] and Esper et al. [37] from Spanish sites.

Whereas bimodality at the Cazorla Natural Park in southern Spain was characterized by a weakened response during mid-summer months from June–August [37], it was less pronounced in the Pyrenees [35], as well as in Corsica, where only one month (July and August respectively) was insignificant. Such bimodal response patterns have only been observed at western Mediterranean sites thus far; eastern Mediterranean sites, such as *SMO* [38,39], as well as MXD chronologies from central [34,63] and northern European regions [32,33], have not been found to exhibit bimodality.

Given the temperature insensitive MXD formation in Morocco [64] and the bimodal temperature signals at the two Spanish sites [35,37], our findings suggest a tendency toward increased seasonal bimodality with decreasing latitude and/or greater aridity throughout the Western Mediterranean. However, additional studies need to be conducted across the region to identify the mechanisms and climatic thresholds responsible for bimodal temperature signals.

The physiological reasons for this lack of response during peak warmth are not yet fully understood but are potentially related to a temperature-decoupled carbohydrate production [37] and/or an effect of summer drought limiting xylogenesis [65,66]. The latter assumption is in line with previous work by Trouet [67], who found the MXD of *P. nigra* to be more sensitive to August precipitation than to temperature at several sites in southern Italy and Greece, whereas Esper et al. [64] reported the MXD formation in xeric regions of Morocco to be primary controlled by drought variability.

Since the high mountain regions of Corsica can also be subject to drought from June–August [13], our results imply that high evapotranspiration rates limit the July–August soil water contents, thus, temporally altering the sensitivity of latewood formation toward precipitation. This hypothesis is supported by dendrometer data obtained along an elevational transect of pines in Corsica revealing fast changes in stem circumference after precipitation events in summer and rainfall-induced cambial reactivation in autumn [68]. The latter might also explain the negative correlations of MXD with September precipitation (Figure S5).

The wood anatomical traits of *P. nigra* latewood, such as the tracheid diameter, lumen width, and cell wall thickness, are strongly determined by the trees' water status, as their expression results from trade-offs between the hydraulic requirements of the xylem and the avoidance of embolism [69–71]. Protecting the trees from cavitation, smaller tracheids with thicker cell walls are formed in summer, while larger tracheids with thinner cell walls are needed to improve hydraulic efficiency [9,72]. Since the trees vascular system can be severely damaged by xylem embolism, cavitation protection appears to be primarily important. Thus, latewood cells tend to be denser in years with higher monthly temperatures and adequate water supply [69,73].

Temperatures at the beginning and end of the growing season appear to have a strong influence on latewood formation, as sufficient precipitation falls in spring and autumn. The positive relationship between April–May temperatures and MXD is likely related to a combination of early snowmelt, reinforced photosynthetic activity, and the production of non-structural carbohydrates prior to the onset of cambial activity [7,35]. In contrast, correlations in September–October demonstrated a direct influence of temperature on secondary cell wall deposition and lignification [73,74]. Although latewood cell formation generally proceeds from July to September, wall thickening and lignification of terminal tracheids can continue into October [7,75,76], leaving discernible imprints in MXD.

Moderate inter-site correlations (Figure 3) and varying temperature correlations at *Asc*, *Tar,* and *Sor* (Figure 6) suggest that the temperature sensitivity of MXD was co-influenced by local site conditions. Since the duration and intensity of summer drought generally decreases with altitude, trees at lower sites generally contain stronger hydroclimatic signals [68,77,78]. This tendency might also impact the reduced temperature correlations at *Tar* (1450 m a.s.l.), as this site is located approx. 150 m beneath *Asc* in the adjacent valley.

The MXD chronology from *Sor* at only 1400 m a.s.l., however, indicates the highest temperature sensitivity, and thus elevational differences appear less influential overall. Previous studies pointed to the combined biogeographical effects of local topography, slope exposure, soil formation, and water availability when discussing signals in Corsican TRW networks [7], tree ring stable isotopes [8,79], and intra-annual density fluctuations [69]. This might also be applicable for MXD; however, further measurements and a network across the island are necessary to disentangle the impact of local site conditions on *P. nigra* MXD formation.

4.3. Fading Temperature Sensitivity

In environments where temperature is the limiting factor of tree growth, MXD has proven ideal for reconstructing past summer temperature variability [33,34,53]. However, hemispheric studies have reported a decreasing temperature sensitivity since the second half of the 20th century [80,81]. This phenomenon, known as the "divergence problem", describes the inability of temperature-sensitive tree-ring chronologies to adequately capture 20th century warming. The lack of mirroring recent warming questions the reliability of tree-ring-derived temperature reconstructions during putative pre-instrumental warm periods.

Despite widespread evidence in a network of MXD data obtained from multiple sites across the Northern Hemisphere [80], divergence appears to be more prevalent at northern latitudes [82]. As most records were developed in the 1980s and 1990s, respectively, and only a few extend until the second decade of the 21st century [80,83], there is a need to update MXD records toward the present for further in-depth-investigations of the divergence problem.

Our Corsican MXD chronologies reveal a similar decoupling from temperature in the late 20th century, resulting in an underestimate of $\geq$1.56 °C between the warmer instrumental and colder reconstructed temperatures in the 21st century. In contrast to the results by Briffa et al. [80,81], this decoupling starts in the late 1990s and not in the 1960s. We suggest that the increasing temperatures throughout recent decades have resulted in more severe summer drought periods with higher evapotranspiration rates at our study sites.

Instrumental observations support this assumption and reveal that warm-season temperatures have continuously increased over the past 100 years, particularly after 1980 CE (Figure 7c). While the AMJJ and SO temperatures from 1980–2000 CE are comparable to those of the 1940s or 1950s, warming amplified rapidly thereafter surpassing nearly all 19th century observations. Since this temperature increase is not accompanied by increasing rainfall, the offset between precipitation and potential evapotranspiration is widening toward the present [84].

Drought episodes have begun to occur more frequently and persist longer, particularly since the 1990s when hydroclimate extreme events were most severe in the Western and

Central Mediterranean [85,86]. In Corsica, the frequency of dry years since intensified rapidly from 20% to 50%, while heavy rainfall events occurred more frequently [84] further promoting summer drought, as water infiltration is impeded by the rocky slopes and large portions of precipitation are lost to surface runoff [68].

We therefore conclude that the *P. nigra* trees growing at the upper treeline have suffered from enhanced drought stress since the 1990s, causing the decrease in MXD sensitivity to warm-season temperatures toward the end of the 20th century. At the same time, running correlations revealed that the June–July precipitation became increasingly important for MXD formation, although the precipitation signals were weak overall. The 1990s are identified as the turning point in MXD climate sensitivity. It appears that the succession of several severe drought events caused a shortage of carbohydrate reserves due to inhibited photosynthetic activity during summer [70,87].

Although Black pines feature an effective stomatal control mechanism [88] and indicate a plastic response to dryness with a rapid recovery thereafter [15], trees at *Tar* have suffered particularly from prolonged drought stress since the 1990s. This could explain the anti-correlations with temperature over the most recent calibration period. The combined effects of high temperatures and low water availability stimulate stomatal closure, limit the absorption of carbon dioxide, and further a shortage of non-structural carbohydrates required for cell wall formation [87,89,90].

This conclusion is consistent with previous dendroclimatological studies detailing drought as an important driver of Mediterranean tree growth and suggesting that the increasing frequency and duration of summer aridity has reduced the temperature-growth relationship at southern European sites [91–95]. The Corsican pine forests are also affected by the regular wildfires characteristic for Mediterranean forests [96,97]. Wildfires have been recognized as disturbance events in dendroclimatic studies as they can leave distinct fingerprints in the tree-ring series of surviving pine trees [98–100].

However, whereas the number of recorded fires increased throughout the 20th century in many Mediterranean regions [101], there was no indication of a change in Corsican fire regime coinciding with the altered climate sensitivity in high elevation MXD data as reported here. The striking coherence among TRW chronologies from multiple Corsican pine sites, extending well into the 21st century [7,9] supports this conclusion that local fire events are of minor importance to the climate signals recorded in tree-ring growth proxies.

Despite possible uncertainties in climate signal estimation emerging from the application of gridded and instrumental station data from the coastal plain, the Corsican composite chronologies contain crucial temperature information, as COR_{HGS} indicated high coherence in low-frequency variability with the world's best replicated (n = 414) MXD record from the Spanish Pyrenees (*GER*). The *GER* chronology correlated significantly ($r_{1950–2014}$ = 0.72, $p < 0.01$) with the May–June and August–September temperatures over large parts of the Western Mediterranean [35].

Similar spatial correlations were recorded between the *ABC200* and AMJJ and SO temperatures prior to 1980 CE. Surprisingly, despite the greater geographical distance, COR_{HGS} was more closely related to a May–September temperature reconstruction based on MXD from Pyrenean mountain pines [36] than to the August–September temperature reconstruction derived from stable carbon isotopes of Corsican Black pines [8]. This discrepancy could result from both the different seasonalities and/or the climate proxies, as the carbon isotopes are more closely influenced by the mutual interactions of temperature, precipitation, and transpiration and carry a mixed climate signal [8].

Based on these findings, we hypothesize that inter-annual MXD variability derived from Corsican Black pines can reliably represent large-scale temperature patterns across the Central-Western Mediterranean over more than 500 years. However, due to the decreasing sensitivity since the late 20th century, a formal reconstruction of past temperatures is not warranted. The development of more and better-replicated MXD chronologies are required to determine how the increasing drought sensitivity affects *P. nigra* growth and to improve our understanding of past climate dynamics in Corsica.

5. Conclusions

By combining 69 MXD measurements from three high-elevation sites in Corsica, we updated previously established density data by 36 years into the 21st century and by 350 years back to the Middle Ages. After applying two detrending techniques that were able to preserve multi-centennial variability, as well as age-band decomposition, all chronologies of the now longest MXD record for the Central-Western Mediterranean indicated similar associations with climate data. The strongest correlations were observed with April–July and September–October temperatures over calibration periods prior to 1980 CE.

August temperatures were found to play a minor role in MXD formation, accentuating a bimodal seasonality in temperature response that is similar to observations at Spanish sites in the Central Pyrenees and Andalusia. The bimodality in temperature sensitivity is likely related to (1) an unimpeded carbohydrate production during mid-summer, when temperatures do not fall below the physiological thresholds; while, at the same time, (2) distinct drought conditions cause stomatal closure inhibiting photosynthetic activity. Comparisons with other temperature-sensitive MXD chronologies from the Mediterranean showed that the Corsican density record contains large-scale climate information over more than 500 years.

However, the weakening temperature associations since the 1990s caused by differing low-frequency trends between wood density and instrumental temperature data raise doubts regarding the reliability of *P. nigra* MXD for climate reconstruction. We demonstrated that the post-1990 CE divergence was likely due to a shift from thermal to hydroclimate forcing. In context of recent warming, our results underline the significance of updating tree-ring density data into the present to evaluate whether MXD-based temperature reconstructions derived from 20th century calibration periods remain valid into the 21st century. For a better understanding of underlying physiological mechanisms and the influence of drought on MXD formation, additional studies of wood anatomical traits would be helpful.

Supplementary Materials: The following are available online at https://www.mdpi.com/article/10.3390/atmos12070804/s1, Table S1: MXD site chronology characteristics; Table S2: MXD composite chronology characteristics; Figure S1: Effects of merging site measurements, Figure S2: Effects of mean adjustment; Figure S3: Sample replication and regional curves of the composite MXD data; Figure S4: Temperature signal estimation using CRU TS4.04 data; Figure S5: Precipitation signal estimation using GPCC v2020 data.

Author Contributions: Conceptualization, P.R., C.H., and J.E.; methodology, P.R. and J.E.; formal analysis, P.R. and J.E.; investigation, P.R., C.H., L.S., A.B., F.H., S.L., F.R., and J.E.; resources, C.H., A.B., S.S., F.H., S.L., U.B., and J.E.; data curation, P.R., C.H., F.R., U.B., and J.E.; writing—original draft preparation, P.R.; writing—review and editing, P.R., C.H., L.S., A.B., S.S., F.H., S.L., F.R., U.B., and J.E.; visualization, P.R. and J.E.; supervision, C.H. and J.E.; project administration, P.R., C.H., and J.E.; funding acquisition, J.E. All authors have read and agreed to the published version of the manuscript.

Funding: This research was funded by the German Research Foundation, Grant No. ES 161/12-1. C.H. received support from the German Research Foundation (HA 8048/1-1), U.B. and J.E. from the ERC Advanced Grant Monostar (AdG 882727).

Data Availability Statement: Data will be made available at the International Tree-Ring Data Bank (https://www.ncdc.noaa.gov/data-access/paleoclimatology-data/datasets/tree-ring) at acceptance.

Acknowledgments: The authors thank Birgit Wöste, Eileen Kuhl, Markus Kochbeck, and Philipp Schulz for laboratory support.

Conflicts of Interest: The authors declare no conflict of interest.

References

1. Diffenbaugh, N.S.; Giorgi, F. Climate change hotspots in the CMIP5 global climate model ensemble. *Clim. Chang.* **2012**, *114*, 813–822. [CrossRef] [PubMed]
2. Gao, X.; Giorgi, F. Increased aridity in the Mediterranean region under greenhouse gas forcing estimated from high resolution simulations with a regional climate model. *Glob. Planet. Chang.* **2008**, *62*, 195–209. [CrossRef]
3. Hertig, E.; Jacobeit, J. Downscaling future climate change: Temperature scenarios for the Mediterranean area. *Glob. Planet. Chang.* **2008**, *63*, 127–131. [CrossRef]
4. Beniston, M.; Stephenson, D.; Christensen, O.B.; Ferro, C.; Frei, C.; Goyette, S.; Halsnaes, K.; Holt, T.; Jylhä, K.; Koffi, B.; et al. Future extreme events in European climate: An exploration of regional climate model projections. *Clim. Chang.* **2007**, *81*, 71–95. [CrossRef]
5. Sánchez, E.; Gallardo, C.; Gaertner, M.A.; Arribas, A.; Castro, M. Future climate extreme events in the Mediterranean simulated by a regional climate model: A first approach. *Glob. Planet. Chang.* **2004**, *44*, 163–180. [CrossRef]
6. Fritts, H.C. *Tree Rings and Climate*, 1st ed.; Blackburn Press: Caldwell, NJ, USA, 1976; ISBN 978-1-930665-39-2.
7. Hetzer, T. Xylem Variability as a Proxy for Environmental and Climate Change in Corsica During the Past Millennium. Ph.D. Thesis, Friedrich-Alexander-University Erlangen-Nürnberg, Erlangen, Germany, 2013.
8. Szymczak, S.; Joachimski, M.M.; Bräuning, A.; Hetzer, T.; Kuhlemann, J. A 560 yr summer temperature reconstruction for the western Mediterranean basin based on stable carbon isotopes from *Pinus nigra* ssp. laricio (Corsica/France). *Clim. Past* **2012**, *8*, 1737–1749. [CrossRef]
9. Szymczak, S.; Hetzer, T.; Bräuning, A.; Joachimski, M.M.; Leuschner, H.-H.; Kuhlemann, J. Combining wood anatomy and stable isotope variations in a 600-year multi-parameter climate reconstruction from Corsican black pine. *Quat. Sci. Rev.* **2014**, *101*, 146–158. [CrossRef]
10. Knerr, I.; Trachte, K.; Garel, E.; Huneau, F.; Santoni, S.; Bendix, J. Partitioning of large-scale and local-scale precipitation events by means of spatio-temporal precipitation regimes on Corsica. *Atmosphere* **2020**, *11*, 417. [CrossRef]
11. Rome, S.; Giorgetti, J.-P. La montagne corse et ses caractéristiques climatiques. *Météorologie* **2007**, *59*, 39–50. [CrossRef]
12. Koninklijk Nederlands Meteorologisch Instituut (KNMI) Climate Explorer. Climate Data from Ajaccio (WMO Station Code 7761) and Bastia (WMO Station Code 7790). Available online: http://climexp.knmi.nl (accessed on 5 October 2020).
13. Rome, S.; Giorgetti, J.-P. Du climat de la montagne corse et ses aléas. In *Les Risques Liés au Temps et au Climat, XIXe Colloque de l'Association Internationale de Climatologie, Épernay, France, 6–9 Septembre 2006*; Beltrando, G., Madelin, M.M., Quénel, H., Eds.; Association Internationale de Climatologie: Épernay, France, 2006; pp. 486–492. ISBN 2-901560-70-9.
14. Médail, F.; Verlaque, R. Ecological characteristics and rarity of endemic plants from southeast France and Corsica: Implications for biodiversity conversation. *Biol. Conserv.* **1997**, *80*, 269–281. [CrossRef]
15. Eilmann, B.; Rigling, A. Tree-growth analyses to estimate tree species' drought tolerance. *Tree Physiol.* **2012**, *32*, 178–187. [CrossRef]
16. Fernández-Pérez, L.; Villar-Salvador, P.; Martínez-Vilalta, J.; Toca, A.; Zavala, M.A. Distribution of pines in the Iberian peninsula agrees with species differences in foliage frost tolerance, not with vulnerability to freezing-induced xylem embolism. *Tree Physiol.* **2018**, *38*, 507–516. [CrossRef]
17. Luterbacher, J.; García-Herrera, R.; Akcer-On, S.; Allan, R.; Alvarez-Castro, M.C.; Benito, G.; Booth, J.; Büntgen, U.; Cagatay, N.; Colombaroli, D.; et al. A review of 2000 years of paleoclimatic evidence in the Mediterranean. In *The Climate of the Mediterranean Region: From the Past to the Future*, 1st ed.; Lionello, P., Ed.; Elsevier Insights: Amsterdam, The Netherlands, 2012; Volume 1, pp. 87–185. ISBN 978-0-12-416042-2.
18. Tintner, J.; Smidt, E. Resistance of wood from Black pine (*Pinus nigra var. austriaca*) against weathering. *J. Wood Sci.* **2018**, *64*, 816–822. [CrossRef]
19. Seim, A.; Treydte, K.; Trouet, V.; Frank, D.; Fonti, P.; Tegel, W.; Panayotov, M.; Fernández-Donado, L.; Krusic, P.; Büntgen, U. Climate sensitivity of Mediterranean pine growth reveals distinct east-west dipole. *Int. J. Climatol.* **2015**, *35*, 2503–2513. [CrossRef]
20. Touchan, R.; Anchukaitis, K.J.; Meko, D.M.; Kerchouche, D.; Slimani, S.; Ilmen, R.; Hasnaoui, F.; Guibal, F.; Camarero, J.J.; Sánchez-Salguero, R.; et al. Climate controls on tree growth in the Western Mediterranean. *Holocene* **2017**, *27*, 1429–1442. [CrossRef]
21. Esper, J.; Konter, O.; Klippel, L.; Krusic, P.J.; Büntgen, U. Pre-instrumental summer precipitation variability in northwestern Greece from a high-elevation *Pinus heldreichii* network. *Int. J. Climatol.* **2021**, *41*, 2828–2839. [CrossRef]
22. Griggs, C.; DeGaetano, A.; Kuniholm, P.; Newton, M. A regional high-frequency reconstruction of May–June precipitation in the north Aegean from oak tree rings, A.D. 1089–1989. *Int. J. Climatol.* **2007**, *27*, 1075–1089. [CrossRef]
23. Ruiz-Labourdette, D.; Génova, M.; Schmitz, M.F.; Urrutia, R.; Pineda, F.D. Summer rainfall variability in European Mediterranean mountains from the sixteenth to the twentieth century reconstructed from tree rings. *Int. J. Biometeorol.* **2014**, *58*, 1627–1639. [CrossRef]
24. Touchan, R.; Meko, D.M.; Aloui, A. Precipitation reconstruction for northwestern Tunisia from tree rings. *J. Arid Environ.* **2008**, *72*, 1887–1896. [CrossRef]
25. Cook, E.R.; Seager, R.; Kushnir, Y.; Briffa, K.R.; Büntgen, U.; Frank, D.; Krusic, P.J.; Tegel, W.; van der Schrier, G.; Andreu-Hayles, L.; et al. Old World megadroughts and pluvials during the Common Era. *Sci. Adv.* **2015**, *1*, e1500561. [CrossRef]
26. Esper, J.; Frank, D.; Büntgen, U.; Verstege, A.; Luterbacher, J.; Xoplaki, E. Long-term drought severity variations in Morocco. *Geophys. Res. Lett.* **2007**, *34*. [CrossRef]

27. Klippel, L.; Krusic, P.J.; Brandes, R.; Hartl, C.; Belmecheri, S.; Dienst, M.; Esper, J. A 1286-year hydro-climate reconstruction for the Balkan peninsula. *Boreas* **2018**, *47*, 1218–1229. [CrossRef]
28. Nicault, A.; Alleaume, S.; Brewer, S.; Carrer, M.; Nola, P.; Guiot, J. Mediterranean drought fluctuation during the last 500 years based on tree-ring data. *Clim. Dyn.* **2008**, *31*, 227–245. [CrossRef]
29. Tejedor, E.; de Luis, M.; Cuadrat, J.M.; Esper, J.; Saz, M.A. Tree-ring-based drought reconstruction in the Iberian range (east of Spain) since 1694. *Int. J. Biometeorol.* **2016**, *60*, 361–372. [CrossRef] [PubMed]
30. Büntgen, U.; Frank, D.; Trouet, V.; Esper, J. Diverse climate sensitivity of Mediterranean tree-ring width and density. *Trees* **2010**, *24*, 261–273. [CrossRef]
31. Esper, J.; Schneider, L.; Smerdon, J.E.; Schöne, B.R.; Büntgen, U. Signals and memory in tree-ring width and density data. *Dendrochronologia* **2015**, *35*, 62–70. [CrossRef]
32. Esper, J.; Frank, D.; Timonen, M.; Zorita, E.; Wilson, R.; Luterbacher, J.; Holzkämper, S.; Fischer, N.; Wagner, S.; Nievergelt, D.; et al. Orbital forcing of tree-ring data. *Nat. Clim. Chang.* **2012**, *2*, 862–866. [CrossRef]
33. Esper, J.; Düthorn, E.; Krusic, P.; Timonen, M.; Büntgen, U. Northern European summer temperature variations over the Common Era from integrated tree-ring density records. *J. Quat. Sci.* **2014**, *29*, 487–494. [CrossRef]
34. Büntgen, U.; Frank, D.C.; Nievergelt, D.; Esper, J. Summer temperature variations in the European Alps, A.D. 755–2004. *J. Clim.* **2006**, *19*, 5606–5623. [CrossRef]
35. Büntgen, U.; Krusic, P.J.; Verstege, A.; Sangüesa-Barreda, G.; Wagner, S.; Camarero, J.J.; Ljungqvist, F.C.; Zorita, E.; Oppenheimer, C.; Konter, O.; et al. New tree-ring evidence from the Pyrenees reveals western Mediterranean climate variability since medieval times. *J. Clim.* **2017**, *30*, 5295–5318. [CrossRef]
36. Dorado-Liñán, I.; Büntgen, U.; González-Rouco, F.; Zorita, E.; Montavez, J.P.; Gómez-Navarro, J.J.; Brunet, M.; Heinrich, I.; Helle, G.; Gutiérrez, E. Estimating 750 years of temperature variations and uncertainties in the Pyrenees by tree-ring reconstructions and climate simulations. *Clim. Past* **2012**, *8*, 919–933. [CrossRef]
37. Esper, J.; Hartl, C.; Tejedor, E.; de Luis, M.; Günther, B.; Büntgen, U. High-resolution temperature variability reconstructed from Black pine tree ring densities in southern Spain. *Atmosphere* **2020**, *11*, 748. [CrossRef]
38. Esper, J.; Klippel, L.; Krusic, P.J.; Konter, O.; Raible, C.C.; Xoplaki, E.; Luterbacher, J.; Büntgen, U. Eastern Mediterranean summer temperatures since 730 CE from Mt. Smolikas tree-ring densities. *Clim. Dyn.* **2020**, *54*, 1367–1382. [CrossRef]
39. Klippel, L.; Krusic, P.J.; Konter, O.; St. George, S.; Trouet, V.; Esper, J. A 1200+ year reconstruction of temperature extremes for the northeastern Mediterranean region. *Int. J. Climatol.* **2019**, *39*, 2336–2350. [CrossRef]
40. Leonelli, G.; Coppola, A.; Salvatore, M.C.; Baroni, C.; Battipaglia, G.; Gentilesca, T.; Ripullone, F.; Borghetti, M.; Conte, E.; Tognetti, R.; et al. Climate signals in a multispecies tree–ring network from central and southern Italy and reconstruction of the late summer temperatures since the early 1700s. *Clim. Past* **2017**, *13*, 1451–1471. [CrossRef]
41. Schweingruber, F.H. NOAA/WDS Paleoclimatology—Schweingruber—Col de Sorba Mount Renoso—PINI—ITRDB FRAN027. NOAA National Centers for Environmental Information. Available online: https://www.ncdc.noaa.gov/paleo-search/study/4389 (accessed on 5 October 2020).
42. Björklund, J.; Von Arx, G.; Nievergelt, D.; Wilson, R.; Van den Bulcke, J.; Günther, B.; Loader, N.J.; Rydval, M.; Fonti, P.; Scharnweber, T.; et al. Scientific merits and analytical challenges of tree-ring densitometry. *Rev. Geophys.* **2019**, *57*, 1224–1264. [CrossRef]
43. Eschbach, W.; Nogler, P.; Schär, E.; Schweingruber, F.H. Technical advances in the radiodensitometrical determination of wood density. *Dendrochronologia* **1995**, *13*, 155–168.
44. Schweingruber, F.H.; Fritts, H.C.; Bräker, O.U.; Drew, L.G.; Schär, E. The X-ray technique as applied to dendroclimatology. *Tree Ring Bull.* **1978**, *38*, 61–91.
45. Cook, E.R.; Krusic, P.J. *Program ARSTAN, A Tree-Ring Standardization Program Based on Detrending and Autoregressive Timeseries Modeling with Interactive Graphics*; Lamont-Doherty Earth Observatory, Columbia University: Palisades, NY, USA, 2005.
46. Cook, E.; Peters, K. Calculating unbiased tree-ring indices for the study of climatic and environmental change. *Holocene* **1997**, *7*, 361–370. [CrossRef]
47. Frank, D.; Esper, J.; Cook, E.R. Adjustment for proxy number and coherence in a large-scale temperature reconstruction. *Geophys. Res. Lett.* **2007**, *34*. [CrossRef]
48. Cook, E.R. A Time Series Analysis Approach to Tree-Ring Standardization. Ph.D. Thesis, University of Arizona, Tucson, AZ, USA, 1985.
49. Wigley, T.M.L.; Briffa, K.R.; Jones, P.D. On the average of correlated time series, with applications in dendroclimatology and hydrometeorology. *J. Appl. Meteorol. Clim.* **1984**, *23*, 201–213. [CrossRef]
50. Esper, J.; Cook, E.R.; Krusic, P.J.; Peters, K.; Schweingruber, F.H. Tests of the RCS method for preserving low-frequency variability in long tree-ring chronologies. *Tree Ring Res.* **2003**, *59*, 81–98.
51. Fang, K.; Gou, X.; Peters, K.; Li, J.; Zhang, F. Removing biological trends from tree-ring series: Testing modified Hugershoff curves. *Tree Ring Res.* **2010**, *66*, 51–59. [CrossRef]
52. Cook, E.R.; Briffa, K.R.; Meko, D.M.; Graybill, D.A.; Funkhouser, G. The 'segment length curse' in long tree-ring chronology development for palaeoclimatic studies. *Holocene* **1995**, *5*, 229–237. [CrossRef]
53. Briffa, K.R.; Jones, P.D.; Bartholin, T.S.; Eckstein, D.; Schweingruber, F.H.; Karlén, W.; Zetterberg, P.; Eronen, M. Fennoscandian summers from AD 500: Temperature changes on short and long timescales. *Clim. Dyn.* **1992**, *7*, 111–119. [CrossRef]

54. Esper, J.; Krusic, P.J.; Ljungqvist, F.C.; Luterbacher, J.; Carrer, M.; Cook, E.; Davi, N.K.; Hartl, C.; Kirdyanov, A.; Konter, O.; et al. Ranking of tree-ring based temperature reconstructions of the past millennium. *Quat. Sci. Rev.* **2016**, *145*, 134–151. [CrossRef]
55. Briffa, K.R.; Osborn, T.J.; Schweingruber, F.H.; Harris, I.C.; Jones, P.D.; Shiyatov, S.G.; Vaganov, E.A. Low-frequency temperature variations from a northern tree ring density network. *J. Geophys. Res. Atmos.* **2001**, *106*, 2929–2941. [CrossRef]
56. Harris, I.; Osborn, T.J.; Jones, P.; Lister, D. Version 4 of the CRU TS monthly high-resolution gridded multivariate climate dataset. *Sci. Data* **2020**, *7*, 1–18. [CrossRef]
57. Schneider, U.; Finger, P.; Rustemeier, E.; Ziese, M.; Becker, A. *Global Precipitation Analysis Products of the GPCC*; Deutscher Wetterdienst (DWD), Abt. Hydrometeorologie, Weltzentrum für Niederschlagsklimatologie: Offenbach am Main, Germany, 2021.
58. Trouet, V.; Van Oldenborgh, G.J. KNMI climate explorer: A web-based research tool for high-resolution paleoclimatology. *Tree Ring Res.* **2013**, *69*, 3–13. [CrossRef]
59. Météo-France Climate Data from Calacuccia Weather Station (20224). Available online: https://meteofrance.com/previsions-meteo-france/calacuccia/20224 (accessed on 7 January 2021).
60. Schweingruber, F.H. NOAA/WDS Paleoclimatology—Schweingruber—Sierra de Crispo—PILE—ITRDB ITAL015. NOAA National Centers for Environmental Information. Available online: https://www.ncdc.noaa.gov/paleo-search/study/4644 (accessed on 5 October 2020).
61. Esper, J.; Cook, E.R.; Schweingruber, F.H. Low-frequency signals in long tree-ring chronologies for reconstructing past temperature variability. *Science* **2002**, *295*, 2250–2253. [CrossRef]
62. Briffa, K.R.; Jones, P.D.; Schweingruber, F.H.; Karlen, W.; Shiyatov, S.G. Tree-ring variables as proxy-climate indicators: Problems with low-frequency signals. In *Climatic Variations and Forcing Mechanisms of the Last 2000 Years*, 1st ed.; Jones, P.D., Bradley, R.S., Jouzel, J., Eds.; Springer: Berlin/Heidelberg, Germany, 1996; Volume 41, pp. 9–41. ISBN 978-3-642-61113-1.
63. Frank, D.; Esper, J. Temperature reconstructions and comparisons with instrumental data from a tree-ring network for the European Alps. *Int. J. Climatol.* **2005**, *25*, 1437–1454. [CrossRef]
64. Esper, J.; Büntgen, U.; Frank, D.; Nievergelt, D.; Treydte, K.; Verstege, A. Multiple tree-ring parameters from Atlas cedar (Morocco) and their climatic signal. In *Schriften des Forschungszentrums Jülich, Reihe Umwelt: TRACE, Tree Rings in Archaeology, Climatology and Ecology*, 4th ed.; Heidrich, I., Gärtner, H., Monbaron, M., Schleser, G., Eds.; Forschungszentrum Jülich: Jülich, Germany, 2006; Volume 61, pp. 46–55. ISBN 978-3-89336-425-1.
65. Camarero, J.J.; Olano, J.M.; Parra, A. Plastic bimodal xylogenesis in conifers from continental Mediterranean climates. *New Phytol.* **2010**, *185*, 471–480. [CrossRef]
66. De Micco, V.; Campelo, F.; De Luis, M.; Bräuning, A.; Grabner, M.; Battipaglia, G.; Cherubini, P. Intra-annual density fluctuations in tree rings: How, when, where, and why? *IAWA J.* **2016**, *37*, 232–259. [CrossRef]
67. Trouet, V. A tree-ring based late summer temperature reconstruction (AD 1675–1980) for the northeastern Mediterranean. *Radiocarbon* **2014**, *56*, 69–78. [CrossRef]
68. Szymczak, S.; Häusser, M.; Garel, E.; Santoni, S.; Huneau, F.; Knerr, I.; Trachte, K.; Bendix, J.; Bräuning, A. How do Mediterranean pine trees respond to drought and precipitation events along an elevation gradient? *Forests* **2020**, *11*, 758. [CrossRef]
69. Hetzer, T.; Bräuning, A.; Leuschner, H.H. High-resolution climatic analysis of wood anatomical features in Corsican pine from Corsica (France) using latewood tracheid profiles. *Trees* **2014**, *28*, 1279–1288. [CrossRef]
70. Martín-Benito, D.; Beeckman, H.; Cañellas, I. Influence of drought on tree rings and tracheid features of *Pinus nigra* and *Pinus sylvestris* in a mesic Mediterranean forest. *Eur. J. For. Res.* **2013**, *132*, 33–45. [CrossRef]
71. Petrucco, L.; Nardini, A.; von Arx, G.; Saurer, M.; Cherubini, P. Isotope signals and anatomical features in tree rings suggest a role for hydraulic strategies in diffuse drought-induced dieback of *Pinus nigra*. *Tree Physiol.* **2017**, *37*, 523–535. [CrossRef]
72. Pittermann, J.; Sperry, J.S.; Wheeler, J.K.; Hacke, U.G.; Sikkema, E.H. Mechanical reinforcement of tracheids compromises the hydraulic efficiency of conifer xylem. *Plant Cell Environ.* **2006**, *29*, 1618–1628. [CrossRef]
73. Fonti, P.; von Arx, G.; García-González, I.; Eilmann, B.; Sass-Klaassen, U.; Gärtner, H.; Eckstein, D. Studying global change through investigation of the plastic responses of xylem anatomy in tree rings. *New Phytol.* **2010**, *185*, 42–53. [CrossRef]
74. Piermattei, A.; Crivellaro, A.; Carrer, M.; Urbinati, C. The "blue ring": Anatomy and formation hypothesis of a new tree-ring anomaly in conifers. *Trees* **2015**, *29*, 613–620. [CrossRef]
75. Lebourgeois, F. Climatic signals in earlywood, latewood and total ring width of Corsican pine from western France. *Ann. For. Sci.* **2000**, *57*, 155–164. [CrossRef]
76. Gričar, J.; Čufar, K.; Oven, P.; Schmitt, U. Differentiation of terminal latewood tracheids in silver fir trees during autumn. *Ann. Bot.* **2005**, *95*, 959–965. [CrossRef] [PubMed]
77. Hartl-Meier, C.; Dittmar, C.; Zang, C.; Rothe, A. Mountain forest growth response to climate change in the northern limestone Alps. *Trees* **2014**, *28*, 819–829. [CrossRef]
78. Häusser, M.; Szymczak, S.; Garel, E.; Santoni, S.; Huneau, F.; Bräuning, A. Growth variability of two native pine species on Corsica as a function of elevation. *Dendrochronologia* **2019**, *54*, 49–55. [CrossRef]
79. Szymczak, S.; Bräuning, A.; Häusser, M.; Garel, E.; Huneau, F.; Santoni, S. The relationship between climate and the intra-annual oxygen isotope patterns from pine trees: A case study along an elevation gradient on Corsica, France. *Ann. For. Sci.* **2019**, *76*, 1–76. [CrossRef]
80. Briffa, K.R.; Schweingruber, F.H.; Jones, P.D.; Osborn, T.J.; Shiyatov, S.G.; Vaganov, E.A. Reduced sensitivity of recent tree-growth to temperature at high northern latitudes. *Nature* **1998**, *391*, 678–682. [CrossRef]

81. Briffa, K.R.; Osborn, T.J.; Schweingruber, F.H. Large-scale temperature inferences from tree-rings: A review. *Glob. Planet. Chang.* **2004**, *40*, 11–26. [CrossRef]
82. D'Arrigo, R.; Wilson, R.; Liepert, B.; Cherubini, P. On the 'divergence problem' in northern forests: A review of the tree-ring evidence and possible causes. *Glob. Planet. Chang.* **2008**, *60*, 289–305. [CrossRef]
83. Schweingruber, F.H.; Briffa, K.R. Tree-ring density networks for climate reconstruction. In *Climatic Variations and Forcing Mechanisms of the Last 2000 Years*, 1st ed.; Jones, P.D., Bradley, R.S., Jouzel, J., Eds.; Springer: Berlin/Heidelberg, Germany, 1996; Volume 41, pp. 43–66. ISBN 978-3-642-61113-1.
84. Laffoley, D.; Baxter, J.; Pergent-Martini, C.; Pergent, G.; Otero, M.M.; Simard, F. *Climate Change and the Marine Environment in Corsica, Report Card 2018*; International Union for Conservation of Nature (IUCN): Gland, Switzerland, 2018.
85. Cook, B.I.; Anchukaitis, K.J.; Touchan, R.; Meko, D.M.; Cook, E.R. Spatiotemporal drought variability in the Mediterranean over the last 900 years. *J. Geophys. Res. Atmos.* **2016**, *121*, 2060–2074. [CrossRef]
86. Spinoni, J.; Naumann, G.; Vogt, J.V.; Barbosa, P. The biggest drought events in Europe from 1950 to 2012. *J. Hydrol. Reg. Stud.* **2015**, *3*, 509–524. [CrossRef]
87. Medrano, H.; Escalona, J.M.; Bota, J.; Gulías, J.; Flexas, J. Regulation of photosynthesis of C_3 plants in response to progressive drought: Stomatal conductance as a reference parameter. *Ann. Bot.* **2002**, *89*, 895–905. [CrossRef]
88. Lebourgeois, F.; Lévy, G.; Aussenac, G.; Clerc, B.; Willm, F. Influence of soil drying on leaf water potential, photosynthesis, stomatal conductance and growth in two black pine varieties. *Ann. Sci. For.* **1998**, *55*, 287–299. [CrossRef]
89. Hartl-Meier, C.; Zang, C.; Büntgen, U.; Esper, J.; Rothe, A.; Göttlein, A.; Dirnböck, T.; Treydte, K. Uniform climate sensitivity in tree-ring stable isotopes across species and sites in a mid-latitude temperate forest. *Tree Physiol.* **2015**, *35*, 4–15. [CrossRef]
90. Olano, J.M.; Linares, J.C.; García-Cervigón, A.I.; Arzac, A.; Delgado, A.; Rozas, V. Drought-induced increase in water-use efficiency reduces secondary tree growth and tracheid wall thickness in a Mediterranean conifer. *Oecologia* **2014**, *176*, 273–283. [CrossRef]
91. Büntgen, U.; Frank, D.; Neuenschwander, T.; Esper, J. Fading temperature sensitivity of Alpine tree growth at its Mediterranean margin and associated effects on large-scale climate reconstructions. *Clim. Chang.* **2012**, *114*, 651–666. [CrossRef]
92. Castagneri, D.; Nola, P.; Motta, R.; Carrer, M. Summer climate variability over the last 250 years differently affected tree species radial growth in a mesic Fagus–Abies–Picea old-growth forest. *For. Ecol. Manag.* **2014**, *320*, 21–29. [CrossRef]
93. Galván, J.D.; Camarero, J.J.; Ginzler, C.; Büntgen, U. Spatial diversity of recent trends in Mediterranean tree growth. *Environ. Res. Lett.* **2014**, *9*, 084001. [CrossRef]
94. Martín-Benito, D.; del Río, M.; Cañellas, I. Black pine (*Pinus nigra* Arn.) growth divergence along a latitudinal gradient in western Mediterranean mountains. *Ann. For. Sci.* **2010**, *67*, 401. [CrossRef]
95. Thiel, D.; Nagy, L.; Beierkuhnlein, C.; Huber, G.; Jentsch, A.; Konnert, M.; Kreyling, J. Uniform drought and warming responses in *Pinus nigra* provenances despite specific overall performances. *For. Ecol. Manag.* **2012**, *270*, 200–208. [CrossRef]
96. Mouillot, F.; Ratte, J.-P.; Joffre, R.; Moreno, J.M.; Rambal, S. Some determinants of the spatio-temporal fire cycle in a mediterranean landscape (Corsica, France). *Landsc. Ecol.* **2003**, *18*, 665–674. [CrossRef]
97. Soulères, O. Les incendies de Haute-Corse. *Rev. For. Fr.* **2000**, *52*, 401–406. [CrossRef]
98. Fulé, P.Z.; Ribas, M.; Gutiérrez, E.; Vallejo, R.; Kaye, M.W. Forest structure and fire history in an old *Pinus nigra* forest, eastern Spain. *For. Ecol. Manag.* **2008**, *255*, 1234–1242. [CrossRef]
99. Szymczak, S.; Bräuning, A.; Häusser, M.; Garel, E.; Huneau, F.; Santoni, S. A dendroecological fire history for central Corsica/France. *Tree Ring Res.* **2020**, *76*, 40–53. [CrossRef]
100. Touchan, R.; Baisan, C.; Mitsopoulos, I.D.; Dimitrakopoulos, A.P. Fire history in European black pine (*Pinus nigra* Arn.) forests of the Valia Kalda, Pindus mountains, Greece. *Tree Ring Res.* **2012**, *68*, 45–50. [CrossRef]
101. Pausas, J.G.; Llovet, J.; Rodrigo, A.; Vallejo, R. Are wildfires a disaster in the Mediterranean basin?—A review. *Int. J. Wildland Fire* **2008**, *17*, 713–723. [CrossRef]